DOI: 10.13009/EUCASS2019-448

Design of Multiple Winglets for Enhancing Aerodynamics in a Micro Air Vehicle.

*A. A. Rodríguez Sevillano *, R. Bardera Mora **, M.A. Barcala Montejano*, E. Barroso Barderas ** and I. Díez Arancibia *.*

** Escuela Técnica Superior de Ingeniería Aeronáutica y del Espacio*

Universidad Politécnica de Madrid.

Plaza del Cardenal Cisneros, 28040 Madrid, Spain. angel.rodriguez.sevillano@upm.es, miguel.barcala@upm.es, i.dieza@upm.es

*** Instituto Nacional de Técnica Aeroespacial (INTA). Carretera de Ajalvir, km 4,5. 28850 Torrejón de Ardoz (MADRID), Spain. barderar@inta.es, barrosobe@inta.es*

Abstract

This paper is focused on designing a Micro Aerial Vehicle (MAV) of biological inspiration at Technical University of Madrid (UPM). The main goal is to analyze a configuration of winglets based on several grids which emulate the wingtip feathers of birds (regimes); it could also be called wing-grid device. In aerospace design, new wingtips tried to modify the lift distribution over the wings; beside this, it is possible to reduce induced drag. The research begins with a wide and extensive analysis in order to decide the optimal configuration of multiple winglets. The computational study has consisted of an optimization using Tornado software in which the number of grids, the chord and the gap between them has been varied. Finally, a model with three grids at the tip of the wing has been the selected solution. Based on this optimal configuration, a complete wind tunnel study using Particle Image Velocimetry (PIV) at National Institute of Aerospace Technology (INTA) facilities has been performed to analyze the feasibility of this wing-grid device.

1. Introduction

In last years, biological inspiration of Unmanned Aerial Vehicle (UAV) designs is one of the greatest challenges inside of aeronautical world. The fast development of bioinspired UAV models has led to emergence of Micro Air Vehicles (MAVs) which are characterized by their small size (dimension less than 600 mm), low flight speed that implies low Reynolds numbers ($10^4 - 10^5$), and low aspect ratios [1]. These models are designed to perform great versatility of tasks in which humans are not able to manage (risky activities, hazardous missions, deep seas operations and unhealthy situations, among others) [2]. Therefore, nowadays, the MAV designs are a challenge of new technologies to find compromise solutions between low Reynolds operating range and low aspect ratio.

Since biologists found the high lift wings of many birds such as hawks, ospreys or vultures with slotted feathers at the ends of their wings, researchers and engineers discovered the reduction of aerodynamic drag while these birds were gliding [3]. In this context, a drag reduction is a really important aspect to consider in the preliminary UAV design due to the great benefits which it produces. Less aerodynamic drag means less fuel to a specific flight and subsequently a lower price is taken into account [4]. For this reason many researchers have been studying how to reduce the induced drag without increasing the wing span of the vehicle. Induced drag is the component of aerodynamic drag which comes from an inevitable consequence of the lift generation of an aircraft passing through the air. As the pressure above the top surface of the wing is lower than the pressure under the wing, the air flow always flows from high pressure regions to low pressure regions. The direct consequence of this process is the generation of a continual swirling of air at the tip of the wing, which is the result of multiple vortices generated from the aircraft wings [5, 6, 7]. Therefore, induced drag is proportional to two variables according to these vortices: radii of the vortices and spacing of them. In this context, many researchers have found that modifying the flow around the wing tips would decrease this component of drag [5, 6, 7]. As a consequence, devices located at the tip of the wings known as ‘’winglets’’ present different configurations. A promising concept which has arose the interest of many engineers has been the biomimetic winglet design. La Roche in 1993 [6] investigated a biomimetic design, known as ‘’wing-grid’’ device, as a solution for separating the vortices and in the same time these vortices would increase its

DOI: 10.13009/EUCASS2019-448

core radii. This first concept was based on several grids located at the tips of the wings and separated from each other a specific dimension which it could simulate the flight of birds. This configuration could resemble to the primary feathers of birds. Therefore, they could be extended or retracted depending on the flight phases in which the vehicle would be. Consequently, the induced drag would be reduced by the wingspan increment [6]. In other words, a rectangular wing produces higher induced drag component than the same wing with wing-grid, both of them with the same wingspan. Some researches of wing-grid device have been performed to verify the real advantages in aerodynamic terms that they could have in flight. Specifically, Bennet in 2001 [8] performed experimental tests in which wing-grid device improved the aerodynamic performances at low values of angle of attack and at velocities up to 27 m/s (values above the critical Reynolds number). Hence, wing-grid device would be effective for cruise, loiter and gliding conditions and they would be retracted in take-off and landing phases. Another studies were focused on attitude control [9,10]. These devices could present the possibility of rolling performance due to a deployment anti-symmetrically. Also, this configuration would be able to perform the control of the UAV with no lift control surface.
This investigation is focused on biomimetic MAV model designed at Technical University of Madrid (UPM), which consists of a model with V-tail and rectangular wing with wing-grid device at the tips of the wing. The model has been designed by using CATIA V5 and has been manufactured by 3D printing. This paper has been divided in two sections. First section based on the preliminary aerodynamic study is dedicated to the computational field: method of panels by means of Tornado software. An optimization of multiple winglets would be carried out. Three variables will be studied: chord, gap and number of winglets; in order to determine the optimal configuration of winglets. Second section is based on experimental tests of the optimal model in order to determine the aerodynamic performance. Wind tunnel tests were carried out at National Institute of Aerospace Technology (INTA) characterizing the flow at different angles of attack; in a range from 0 to 25 degrees with a step of 5 degrees and at different configurations: base model, without winglets (wing-grid retracted) and optimal model with winglets (wing-grid extended).

2. Base UAV model

The base model was designed and manufactured at Technical University of Madrid (UPM) which is located in Madrid (Spain). Its geometry consist of rectangular wing and V tail vertical stabilizer. Both of them have Eppler 186 airfoils, which its form is presented in Figure 1. Rectangular wing was chosen as the best option to install the future wing-grid device to the wings of the UAV due to the studies developed by La Roche [7]. As the grids are based on the primary feathers of birds, the geometry of the vertical stabilizer was also chosen based on the constitution of birds. Therefore, the final UAV model (Section 3.1) will be designed according to the criteria of biological inspiration.

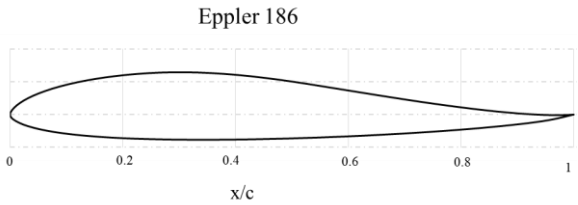

Figure 1: Eppler 186 airfoil geometry.

The base model presents the following geometrical features: the aspect ratio AR is 6 ($AR = \frac{b^2}{S_w}$), the wing span b is 540 mm, the chord c is 90 mm and the wing area S_w is 48600 mm^2.

The model was created with "CATIA V5" software in order to manufacture it by 3D printing. Due to the dimensions of this machine, the model had to be printed in two half-models. The additive material chosen was Acrylonitrile Butadiene Styrene (ABSplus) due to its low price and high finishing quality. Figure 2 shows the front and lateral views of the base model.

Figure 2: Views of Base UAV model (front view on the left and lateral view on the right).

DOI: 10.13009/EUCASS2019-448

3. Computational study

In this section, the computational study of the base UAV model detailed above will be described in order to find the optimal configuration of the multiple winglets. An optimization of three variables have been carried out by means of Tornado software. Tornado software is based on the potential aerodynamics theory and it is implemented by the panel method. The chosen variables were the number of winglets, the gap between them and their chord.

The aerodynamic parameters which will be studied are: maximum aerodynamic efficiency $\left(\frac{C_L}{C_D}\right)_{max}$, required minimum power parameter for maximum endurance in a propeller $\frac{(C_L)^{3/2}}{C_D}$, lift curve slope ratio $\frac{C_{L\alpha}}{2\pi}$ and lift coefficient dimensionless by weight coefficient $\left(\frac{C_L}{C_w}\right)_{max}$. The lift C_L and drag C_D coefficients are defined in equations (1) and (2), respectively:

$$C_L = \frac{L}{\frac{1}{2}\rho V^2 S} \tag{1}$$

$$C_D = \frac{D}{\frac{1}{2}\rho V^2 S} \tag{2}$$

Where *L* and *D*, are the lift and drag forces, respectively; ρ is the flow density, *S* is the wing area of the base model and *V* the velocity.

Numerical tests have been performed at different angles of attack α, from -10º to 10º with an angle step of 1º. The numerical parameters for the simulation are given in the following table:

Table 1: Main design parameters.

Parameters	**Value**
Airfoil Type	Eppler 186
Chord	0.09
VLM method	Tornado
Location of panels	Lineal
Number of panels	1000
Velocity (TAS)	25 m/s
Maximum angle of attack	10º
Minimum angle of attack	-10º
Angle step	1º

The first simulation was based on obtaining the aerodynamic parameters $\left(\frac{C_L}{C_D}\right)_{max}$, $\frac{(C_L)^{3/2}}{C_D}$, $\frac{C_{L\alpha}}{2\pi}$ and $\left(\frac{C_L}{C_w}\right)_{max}$ by varying the number of winglets (NWG) and the gap between them.

Figure 3 and Figure 4 show the maximum aerodynamic efficiency $\left(\frac{C_L}{C_D}\right)_{max}$ and the required minimum power parameter $\frac{(C_L)^{3/2}}{C_D}$ depending on those variables, respectively. The peak of maximum $\left(\frac{C_L}{C_D}\right)_{max}$ and $\frac{(C_L)^{3/2}}{C_D}$ which is the yellow region is obtained for the configuration with 6 winglets and a gap between them of 0.11%. Besides, it is important to notice that there are high values of aerodynamic efficiency $\left(\frac{C_L}{C_D}\right)_{max}$ for configurations with high number of winglets, from 3 to 6 winglets, and with a gap interval of 0.02 – 0.08 % (Figure 3).

DOI: 10.13009/EUCASS2019-448

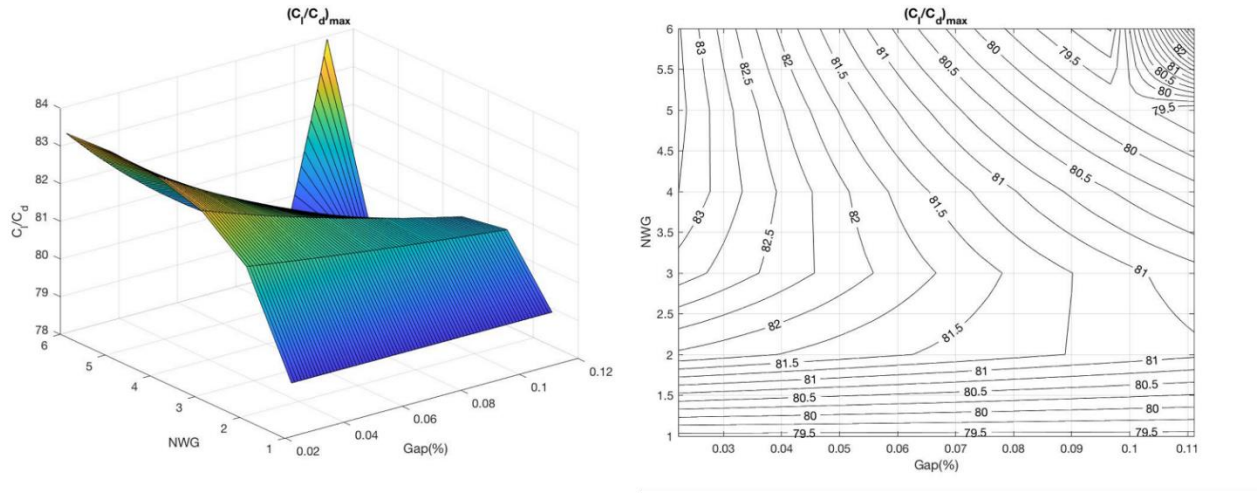

Figure 3. Maximum aerodynamic efficiency $\left(\frac{C_L}{C_D}\right)_{max}$ depending on number of winglets and gap between them.

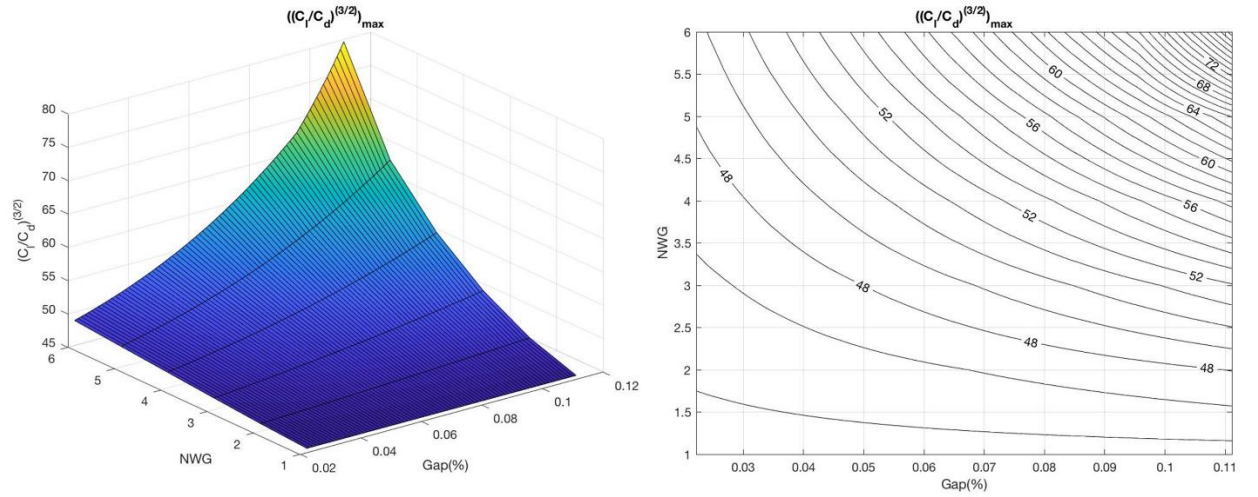

Figure 4. Required minimum power parameter $\frac{(C_L)^{3/2}}{C_D}$ depending on number of winglets and gap between them.

Figure 5 shows the lift curve slope ratio $\frac{C_{L\alpha}}{2\pi}$ according to the number of winglets and the gap between them. The lift curve slope $C_{L\alpha}$ is dimensioned by the lift coefficient of a flat plate which is $C_L = 2\pi\alpha$. The yellow region shows the valid configurations of winglets along with the proper gap. In that region, the lift coefficient slope $C_{L\alpha}$ is higher than the value for the flat plate ($C_L = 2\pi\alpha$) reaching values of $\frac{C_{L\alpha}}{2\pi}$ equal to1.15. However, the blue region represents the value of the lift coefficient slope which is less than the corresponding value for the flat plate. The valid configurations are: any number of winglets with a gap lower than 0.06% and any value of gap with a number of winglets equal to 3 or lower.

Figure 6 represents the lift coefficient dimensioned by the weight coefficient $\left(\frac{C_L}{C_W}\right)_{max}$ according to the number of winglets and the gap between them. As in the previous case, the valid configurations would be embraced in the yellow area. In that region, the value of $\left(\frac{C_L}{C_W}\right)_{max}$ is 20. In this case, the valid configurations would be any number of winglets with a gap lower than 0.08% and any value of gap with a number of winglets equal to 3 or lower.

DOI: 10.13009/EUCASS2019-448

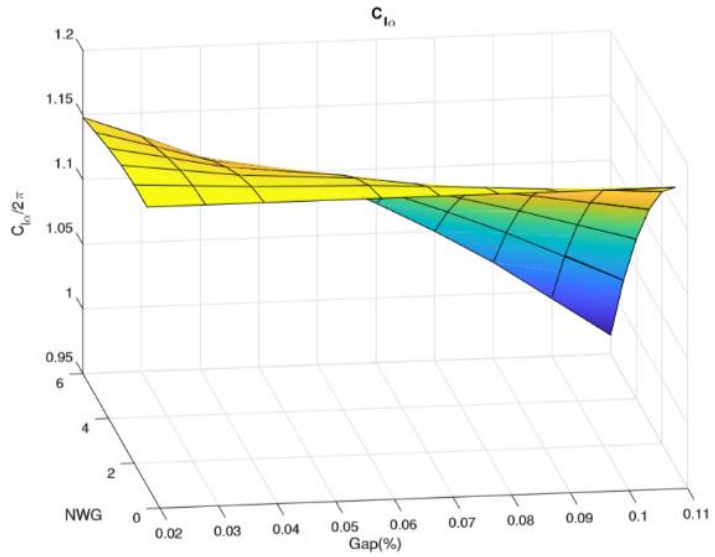

Figure 5. Lift curve slope ratio $C_{L\alpha}/2\pi$.

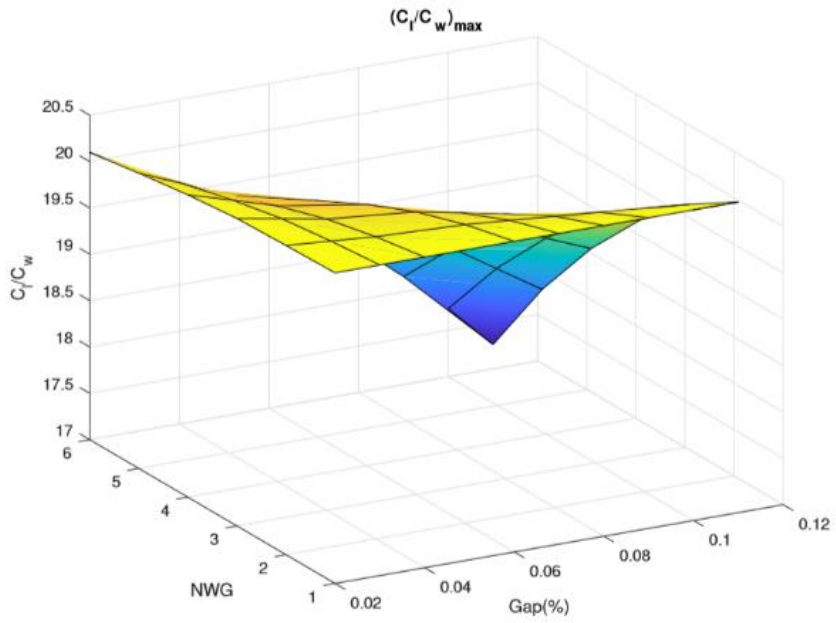

Figure 6. Lift coefficient dimensionalized by weight coefficient $\left(\frac{C_L}{C_W}\right)_{max}$.

The second optimization consisted in obtaining the polar curve (C_L vs C_D) and the C_L vs α for a fixed relation of gap/chord equal to 0.09 (Figure 7). This value has been chosen due to the restrictions of 3D printing machine. By increasing the angle of attack, the lift coefficient grows. Therefore, the strength of vortices generated by the tip of the wing will increase and thus induced drag component.

DOI: 10.13009/EUCASS2019-448

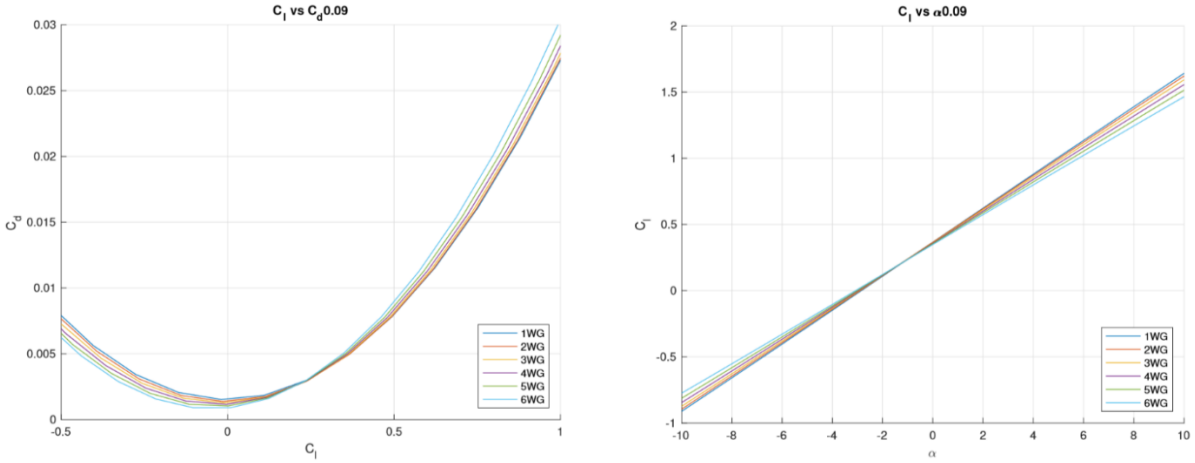

Figure 7. Polar curve (left) and Cl vs α (right) for a relation gap/chord=0.09.

The computational results show that the aerodynamic parameters tend to be more optimal by increasing the number of winglets. In this context, the configuration of 6 winglets would be the best option but the authors have decided to choose the configuration of 3 winglets. This decision has been taken due to some restrictions.
Firstly, the computational study has been developed on the basis of the chord of the wing which is 9 cm. Therefore, the configurations of 4 winglets or more would require a chord dimension of 1.5 cm or lower. The best aerodynamic configuration, 6 winglets, would require a chord of less than 1cm. On the other hand, the 3D printing machine has a physical limitation of manufacturing. The manufacturing of the multiple winglets must be done with enough stiffness to be able to support the experimental test in the wind tunnel. At this point, it is not possible to manufacture the configuration of 6 winglets with enough stiffness due to the required dimensions of them. Therefore, taking all of this into account, the multiple winglets configuration will be the configuration of 3 winglets.
Notice that if the chord dimension were the double, the configuration of high number of winglets could be manufactured. Besides, the chord dimension of the wing would have to be redesign. All of this would be interesting for future studies.

3.1 Optimal model

Once the optimal configuration of multiple winglets is achieved, the next step is to manufacture them in order to test the final UAV model in the Low Speed Wind Tunnel at INTA facilities. The wing-grid system have been designed with CATIA V5 and manufactured by means of 3D printing (same as base model). Figure 8 shows the design of the rectangular wing with the 3 winglets in CATIA.

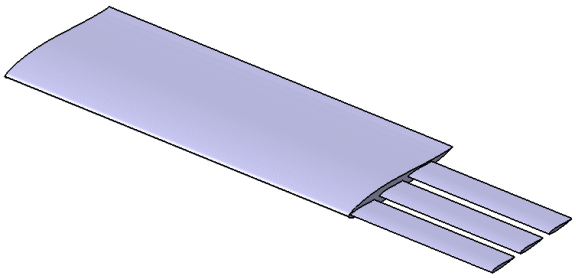

Figure 8: Rectangular wing with 3 winglets in CATIA V5.

The final model has winglets at the tips of the wings which consists of three small semi-wings with the same airfoil as rectangular wing, an Eppler 186 airfoil. The 3 winglets at the wing tip are separated from each other a gap of 4.5 mm between them. The chord of the winglets $c_{winglet}$ is 20 mm and its wing span $b_{winglet}$ is 90 mm. In Figure 9 can be seen the dimensions of the wing-grid system, which are given in mm. These semi-wings have the same angle of

DOI: 10.13009/EUCASS2019-448

attack α as the wing and with zero sweep angle without twist. Figure 8 shows the front view of the final UAV model along with the dimensions of the winglets. The geometrical features of this model are: the aspect ratio of the final model AR' is 8, the wingspan of the final model b' is 720 mm, and the wing area of the final model $S_w{}'$ is 64800 mm^2.

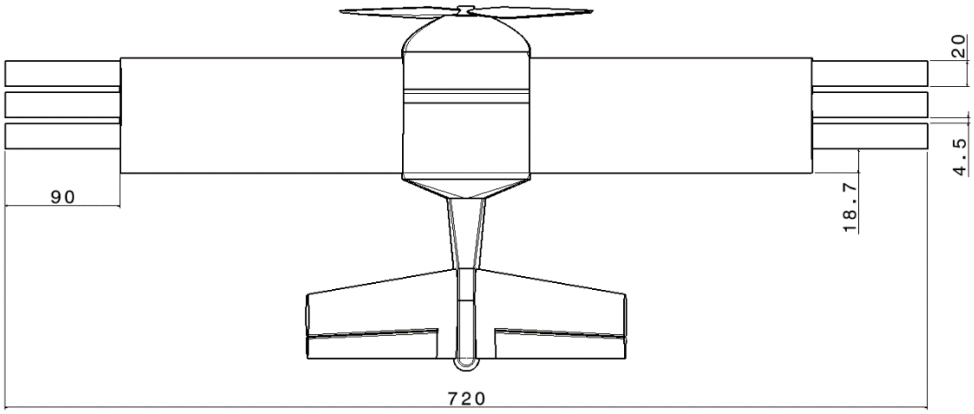

Figure 9: Front view of the optimal UAV configuration. (Dimensions in mm).

Although this paper is focused on the preliminary phase of the UAV model design, there is a requirement to know how this UAV model would be implemented in a future project in order to develop it for real flight. Therefore, all parts of the model have been designed with CATIA. First of all, the volume space has been designed according to the required space to adjust the grids when they have to be retracted. An engine situated inside of the UAV fuselage has the function to move the grids in order to extend or retracted them. Moreover, due to the small size of this model, a tractor propeller can be installed as it can be seen in Figure 10. This tractor propeller will require an electrical engine. As it was described above, this UAV model with multiple winglets could reduce the aerodynamic drag because of the gaps between the small semi-wings which produce a decrement in the size of the vortices created by the tips of the wings. As the same time, these grids would be expected to improve the aerodynamic efficiency of the UAV model due to the increase of the wingspan which it will produce a decrease in induced drag. Another advantage of the development of this UAV model is the possibility to create flight performances with no conventional surface control. Eventually, multiple winglets would be expected to perform rolling control.

Figure 10: Final UAV model with wing-grid device (3 winglets).

4. Experimental Study

In this section, the experimental study will be explained. The wind tunnel facility, the experimental technique, experimental set-up and tests will be described.

DOI: 10.13009/EUCASS2019-448

4.1 Wind Tunnel

The experimental investigation was carried out at National Institute of Aerospace Technology (INTA) facilities which is placed in Spain (Madrid). The INTA nº1 Tunnel is a low speed wind tunnel which has a close circuit and an elliptical open test section of 2000 x 3000 mm^2. The test section is designed with a moving platform which permits modifying the experimental set ups when it will be required. This platform is constructed with streamlined leading and trailing edges to minimize any possible perturbation in the wind tunnel airflow. The facility has a DC engine of 450 kW which works at 420 V and it is located at the opposite side of the working section. The maximum airflow velocity which can achieve this tunnel is 60 m/s and its turbulence intensity is lower than 0.5%.

4.2 Particle Image Velocimetry

Particle Image Velocimetry (PIV) technique was utilized to acquire the velocity field of the final UAV model (Wing-grid). PIV is a planar (2D) non-intrusive technique which measures instantaneously the velocity of tracer particles transported by the air flow. This technique requires of air compressors, a Laskin atomizer, two neodumium-doped yttrium aluminium garnet (*Nd:YAG*) lasers, an optics system which is composed of spherical and cylindrical lenses, a recording system which is a CCD camera, a synchronizer and a post-processing system.
PIV technique is based on flow images analysis, therefore the air flow has to be seeded with tracer particles of olive oil which its diameter is *1 μm* and they are generated by the Laskin atomizer. The pressure of the compressors must be suitable in order to maintain the diameter of the oil particles. Two *Nd:YAG* lasers were required in order to illuminate the tracer particles and its pulses (*190 mJ*) were applied with an interval of time of *22 μs*. To record the laser pulses on images of flow, a high resolution CCD camera with 2048 x 2048 pixels was used (*Nikon Nikkor 50 mm 1:1.4D*). The frequency applied was 10 Hz. The field of view (FOV) of the Nikon Nikkor camera was $420 \text{ x } 420\ mm^2$. Flow images were divided into interrogation windows of 32 x 32 pixels to be able to process the images recorded by the CCD camera. To determine the average particles displacement in these windows, a statistical correlation implemented by Fast Fourier Transform (FFT) has to be applied. With the Nyquist sampling criteria, the interrogation windows could be overlapped by 50%. By means of the Gaussian interpolation, the correlation peak can be adapted to the subpixel accuracy [11]. Last step was applying a post processing algorithm which was able to remove spurious vectors and filled them with valid data. A local mean filtered function with 3 x 3 pixels as a window size was required to complete the experimental process

4.3 Experimental set-up and tests.

The experimental tests consisted of measuring the velocity field at 2/3 of the wing. The two model configurations were studied at different angles of attack in order to determine the aerodynamic performances: model with winglets retracted and model with winglets extended. A total of 6 angles of attack were taken into account, from 0º to 25º with an interval of 5º. All tests were conducted with a free stream velocity of the wind tunnel of 10 m/s which implies a Reynolds number of 6.2×10^4 based on the chord of the wing which is 90 mm.
As it can be seen in Figure 10, the UAV model and wood board had to be painted in black to avoid possible reflections from PIV sheet laser. UAV model had to be attached to the wood board by using a streamlined support strut in order to minimize velocity perturbations. The CCD camera was situated perpendicular to the x-axis of the wind tunnel. A total of 100 pairs of images were taken in all experimental tests by means of CCD camera to visualize the flow. Figure 11 shows the final experimental set-up of the UAV model with winglets.

DOI: 10.13009/EUCASS2019-448

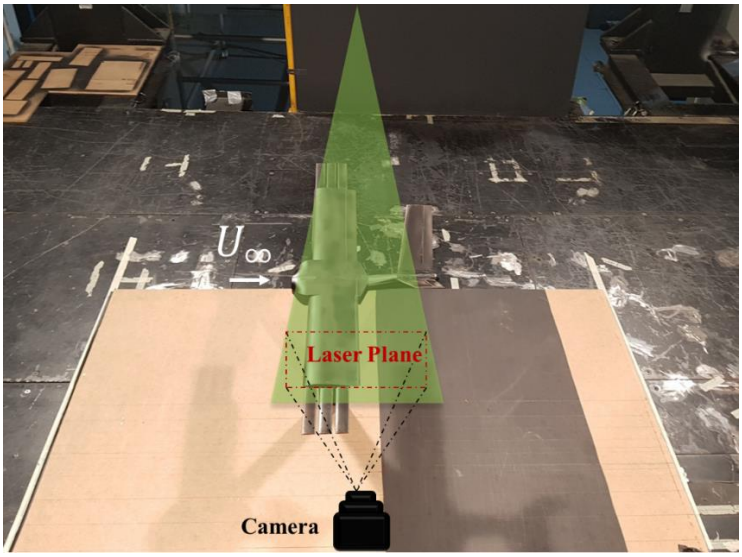

Figure 11: Experimental set-up of final configuration of the *wing-grid.*

5. Discussion and Results

In this section, the experimental results obtained by means of PIV technique will be discussed. PIV measurements will be presented in classical PIV maps according to non-dimensional variables, which will be defined below.
The non-dimensional velocity, V is defined by the following expression (3) as,

$$V = \frac{\sqrt{u^2 + v^2}}{U_\infty} \tag{3}$$

Where U_∞ is the free stream velocity in x direction, and u and v are the velocity components in x and y direction, respectively.
The second dimensionless variable, turbulence intensity, TI can be written as (4),

$$TI = \frac{\sqrt{\sigma_x^2 + \sigma_y^2}}{U_\infty} \tag{4}$$

Where σ_x and σ_y are the standard deviation of the u and v velocity components, respectively.

Figure 12 and 13 show the non-dimensional velocity and the turbulence intensity maps of the two model configurations, winglets retracted and winglets extended, respectively; and at each angle of attack which was defined in a previous section.
Figure 12 shows all non-dimensional velocity maps in both configurations. An orange area can be observed in all of them which represents the free stream velocity of the wind tunnel of 10 m/s. Besides, there is another region above the wing (red area) in which the flow is accelerated by 20% of the free stream velocity. Streamlines have been plotted in order to visualize the flow structure. A region of low velocities represents the wake structure which is generated by the UAV wing. That region at low angles of attack, between 0º and 10º, implies a velocity decrement up to 2 m/s (green region). In this case the structure of the wake remains thin. However, from the angle of attack of 15º flow is detached and the velocities of that region have significantly decreased generating a recirculation bubble (blue area) in which the values of velocity are near to zero. The structure of the recirculation bubble can be seen due to the plotted streamlines.

Notice that the model with winglets extended presents worse adverse effect at high angles of attack than the model with winglets retracted. For this reason, these devices are not recommended for landing and take-off maneuvers. The generation of stall with winglets extended occurs earlier than winglets retracted. In this context, the massive flow detachment with winglets extended takes place at angle of attack of 15º. However with the winglets retracted this phenomena starts at angle of attack of 20º.
Velocity fluctuations regions can be seen in Figure 13 by means of turbulence intensity maps. High turbulence regions can permit knowing what the areas are with flow detachment. The highest values of turbulence intensity are generated from an angle of attack equal to 15º (red region). This could be associated with high drag component.
These results have showed a better aerodynamic performance with winglets retracted at high angles of attack. Therefore, the winglets should be retracted in take-off and landing maneuvers and extended in cruise conditions.

DOI: 10.13009/EUCASS2019-448

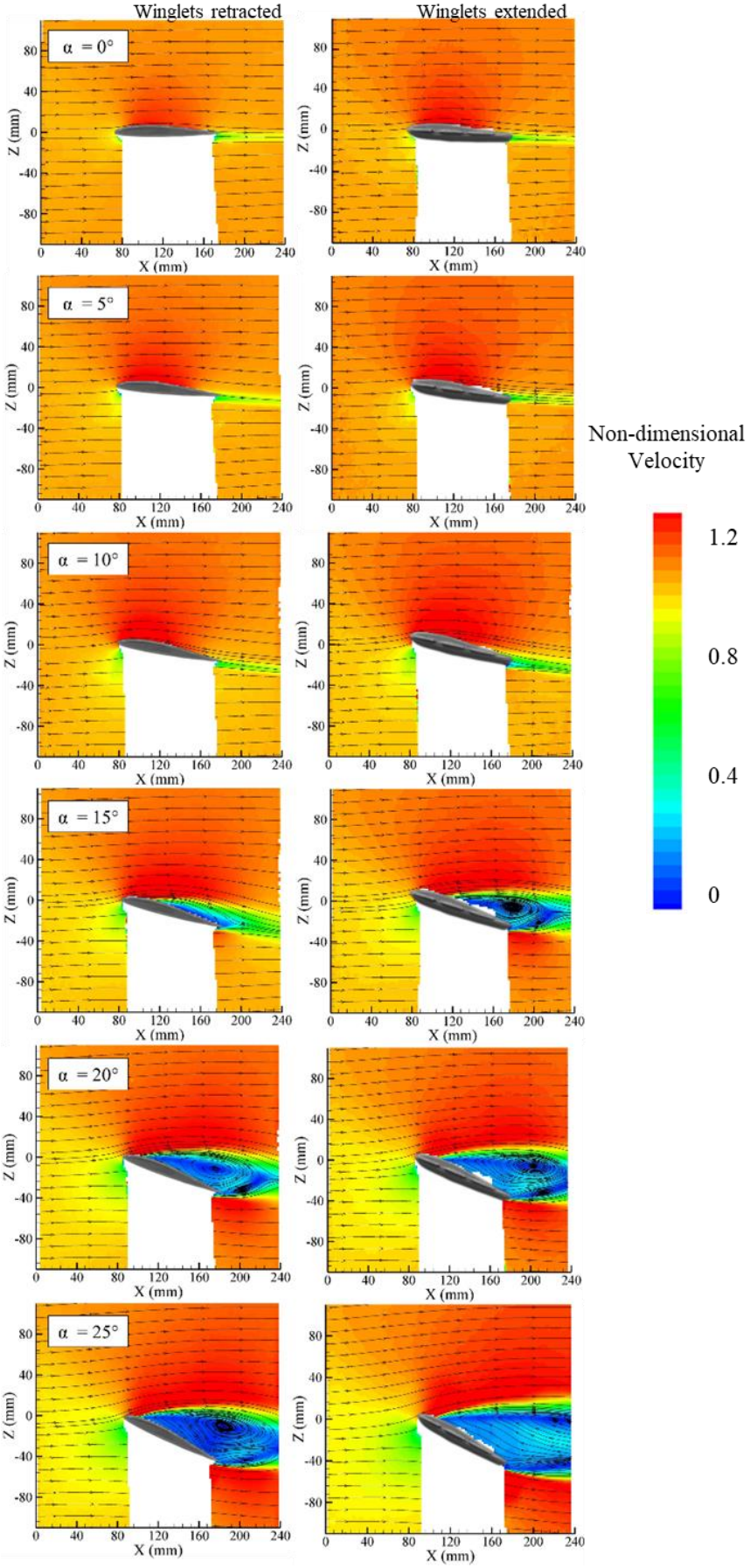

Figure 12: Non-dimensional velocity maps with winglets retracted and extended.

DOI: 10.13009/EUCASS2019-448

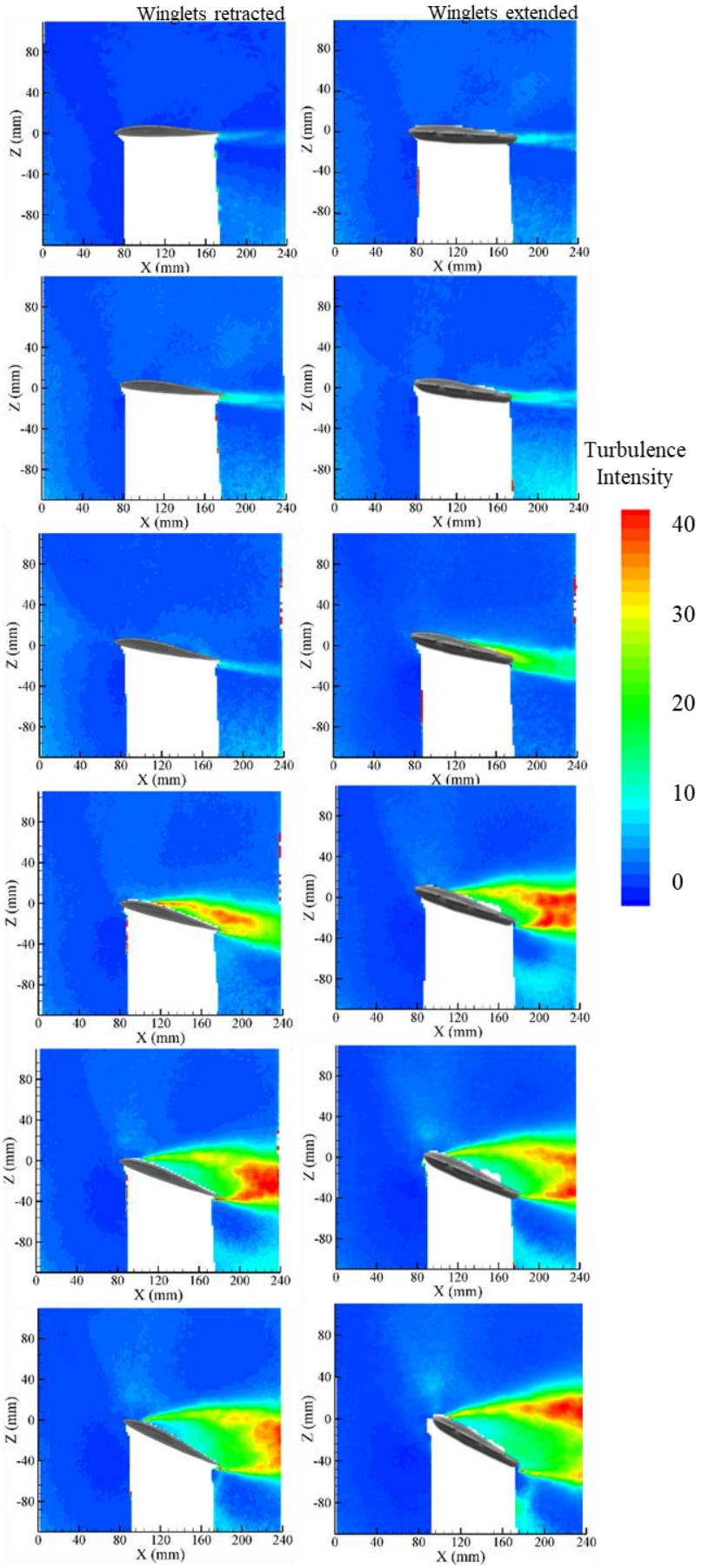

Figure 13: Turbulence intensity maps with winglets.

DOI: 10.13009/EUCASS2019-448

6. Conclusions

Biomimetic Unmanned Aerial Vehicles are characterized for imitating the flight of birds. Due to their reduced geometry, low flight speed and low aspect ratios, these vehicles have become the focus of new technologies for many interesting activities in which the human being is unavailable to perform them (risky activities, hazardous missions, deep seas operations and unhealthy situations). As drag is one of the greatest drawbacks which limits the aerodynamic performance of an aircraft, new UAV designs is resulting from nature observation which will permits a reduction of drag without increasing the wing span.

The studied UAV model in this research is the result of a preliminary design in which an optimization of multiple winglets have been carried out by using Tornado software. This computational task was performed at Technical University of Madrid (UPM). The studied variables were: chord, gap and number of winglets. Computational results were represented in the aerodynamic coefficients in order to determine the optimal configuration. This configuration was based on 3 winglets of grids with a chord of 20 mm and a gap of 4.5 mm.

The final model which is based on rectangular wing with those 3 semi-wings and V-tail was designed and manufactured at Technical University by means of CATIA software and 3D printer, respectively. Following, an experimental tests were carried out at INTA facility. Two configuration were studied at several angles of attack (from 0º to 25º degrees): model with winglets retracted and winglets extended.

Experimental tests were performed in the closed wind tunnel. Particle image velocimetry was used for measuring the velocity field at 2/3 of the half-wing span. The model with winglets extended has a higher massive detachment flow at high angles of attack, from angle of attack of 15º on, producing a very turbulent flow in the near wake of the model. However, the stall generation with winglets extended starts later, at $\alpha = 20º$. Therefore, the winglets would have to be extended in cruise phase while in take-off and landing maneuvers should be retracted.

References

[1] Torres, G. E., & Mueller, T. J. (2004). Low aspect ratio aerodynamics at low Reynolds numbers. *AIAA journal*, *42*(5), 865-873.

[2] Rodriguez Sevillano A.A, Barcala Montejano M.A., Bardera Mora R., '' Biomimetic micro air vehicle controlled by winggrods''. Paper presented at the 8th Conference on Smart Structures and Materials, SMART 2017 and 6th International Conference on Smart Materials and Nanotechnology in Engineering, SMN 2017, 2017 January 413-423.

[3] Tucker, V. A. (1993). Gliding birds: reduction of induced drag by wing tip slots between the primary feathers. *Journal of Experimental Biology*, *180*(1), 285-310.

[4] Kroo, I. (2001). Drag due to lift: concepts for prediction and reduction. *Annual Review of Fluid Mechanics*, *33*(1), 587-617

[5] Smith, M., Komerath, N., Ames, R., Wong, O., & Pearson, J. (2001). Performance analysis of a wing with multiple winglets. In *19th AIAA Applied Aerodynamics Conference* (p. 2407).

[6] Soltani

[7] La Roche, U. y La Roche, H. L. (2004): "Induced Drag Reduction Using Multiple Winglets, Looking Beyond the Prandtl-Munk Linear Model". AIAA Paper No. AIAA-2004-2120

[8] Bennett, D. (2001). The Wing Grid: A New Approach to Reducing Induced Drag.

[9] Jones, K. D., Bradshaw, C. J., Papadopoulos, J., & Platzer, M. F. (2005). Bio-inspired design of flapping-wing micro air vehicles. *The Aeronautical Journal*, *109*(1098), 385-393.

[10] Barcala-Montejano, M. A., Rodríguez-Sevillano, A., Crespo-Moreno, J., Bardera Mora, R., and Silva-González, A. J. "Optimized performance of a morphing micro air vehicle." Unmanned Aircraft Systems (ICUAS), 2015 International Conference pp. 794-800. IEEE Journal of Intelligent Material Systems and Structures.

[11] Adrian, R. J. Particle-imaging techniques for experimental fluid mechanics. Annual Review of Fluid Mechanics 1991, 23: 261-304.